Earthquake Engineering and Engineering Seismology
Volume 2, Number 1, March 2000, pp. 1–21

Strong Ground Motion Characteristics of the Chi-Chi, Taiwan Earthquake of September 21, 1999

Yi-Ben Tsai [1] Ming-Wey Huang [2]

1) *Professor, Institute of Geophysics, National Central University, Chung-Li, Taiwan 32054, R.O.C.*

2) *Graduate student, Institute of Geophysics, National Central University, Chung-Li, Taiwan 32054, R.O.C .*

ABSTRACT

The Chi-Chi, Taiwan earthquake produced a rich set of 422 strong ground motion recordings. In this paper we present some results from our analysis of these recordings. First, we found that the overall level of the observed horizontal peak ground acceleration (PGA) values was relatively low (about 50% less) when compared with what would be predicted for an earthquake of the same magnitude by existing attenuation models based on worldwide data. High horizontal PGA values at sites on the hanging wall and within 20km of the surface fault ruptures are notable exceptions. The horizontal PGA values are indistinguishable among the four different site classes. However, the horizontal PGA values in Taipei Basin, Ilan Plain, and Hwalien area are significantly higher than the average at similar distances. The vertical PGA values on the average are about 0.6 times their horizontal counterparts. Unlike the horizontal PGA, the observed horizontal peak ground velocity (PGV) values are relatively high (about 80% higher) when compared with what would be predicted for an earthquake of the same magnitude by an existing PGV at- tenuation model based on worldwide data. In summary, as far as peak ground motion parameters are concerned, the Chi-Chi earthquake may be called a high-PGV, low-PGA (HV-LA) earthquake. Next, we analyzed the 5% damped acceleration response spectrum shapes for the four different site classes B, C, D, and E, in order to study possible dependence of the response spectrum shape on local geologic site conditions. It is found that the peak spectral amplification factor ranges between 2.3 and 2.5 for all four classes of site conditions. In general, the response spectrum shape for Class B sites on soft rocks older than the Pliocene age has spectral amplification for periods up to about 1.5 seconds. The spectral amplification of Classes C and D sites on stiff soils occurs over periods up to about 2.0 seconds. The spectral amplification of Class E sites on soft soils occurs over periods up to about 3.0 seconds. The response spectrum shapes for Taipei Basin and Ilan Plain are quite similar to Class E sites, whereas Hwalien area is similar to Class C or D sites. Finally, we analyzed the observed characteristics of acceleration response spectra from 44 near-fault sites. For the eight sites within 2km from the surface fault ruptures, the median horizontal PGA value is about 0.5g. The corresponding spectral peak is about 1.0g. The median-plus-one- standard-deviation horizontal PGA value is about 0.7g and the corresponding spectral peak is about 1.8g. Thus, for sites within 2km from the surface fault ruptures, application of a scaling factor of 1.5 to the current seismic design spectrum anchored at a PGA value of 0.33g for Zone 1A appears to be appro- priate. For the 18 sites located at 2 to 10km from the surface fault ruptures, the median horizontal PGA value is about 0.25g. The corresponding peak spectral value is about 0.6g. The median-plus-one-standard-deviation horizontal PGA value is about 0.4g and the corresponding peak spectral value is about 0.8g. Thus, for sites between 2 and 10km from the surface fault ruptures, the current seismic design spectrum anchored at a PGA value of 0.33g for Zone 1A appears to be adequate. For the 33 sites at 10 to 20km from the surface fault ruptures, the median horizontal PGA value is about 0.18g and the corresponding peak spectral value is about 0.45g. The median-plus- one-standard-deviation horizontal PGA value is about 0.3g and the corresponding peak spectral value is about 0.7g. Thus, for sites located between 10 and 20km from the surface fault ruptures, the current seismic design spectrum anchored at a PGA value of 0.33g for Zone 1A is more than adequate.

INTRODUCTION

A disastrous earthquake struck central Taiwan at 01:47 of September 21, 1999 (Taiwan local time). The Seismology Center of the Central Weather Bureau (CWB) located the epicenter at 120.82°E, 23.85°N near the town of Chi-Chi, Nantou County. The focal depth was 8km [1]. The reported magnitude of this earthquake was M_L 7.3 (CWB) and M_W 7.7 (Harvard CMT), respectively. The earthquake has caused heavy casualties and building damages. As of November 26, 1999, 2,432 persons were known killed, 657 persons seriously injured, 46 persons still missing, and 49,542 dwellings totally collapsed, 42,746 dwellings partially collapsed [2]. In addition, there were widespread destruction and disruption of lifelines, including roads and bridges, railroads, communication, water, gas and electric power systems, as shown in Table 1. These lifeline failures had brought great sufferings to the people in the impacted areas. Sadly to say, this was the most damaging earthquake to hit modern Taiwan.

Immediately following the earthquake, the National Science Council mobilized more than 1,200 scientists and engineers to conduct systematic field surveys and to analyze scientific data in order to learn as much as possible from this disastrous event. The lessons learned will be applied not only in the reconstruction of the impacted areas, but also to other areas of similar seismotectonic and man-made environments.

On a somewhat positive note, the earthquake has also left us with a great deal of valuable information and data that can be analyzed and used to reduce potential losses of future earthquakes both in Taiwan and abroad. One notable case in point was that the earthquake produced a very rich set of 422 strong ground motion recordings [3]. In this paper we present some results from our analysis of these recordings. Potential implications for engineering applications will also be discussed.

Table 1 Lifeline Damages from the Chi-Chi Earthquake

A. Electric power supply

Facility	Number
Hydro-power stations	7
Thermal power stations	2
Transformer stations	
1. 345 kv	5
2. 161 kv	6
3. 69 kv	13
Transmission lines	
1. Major switchyard	1
2. Circuits	
345kv	28
161kv	30
69kb	21
3. Towers	
345 kv	355
161 kv	155
69 kv	83
Distribution lines	
1. Power poles	
Broken	678
Fallen	773
Tilted	2,571
2. HV switches	164
Underground switches	44
3. Main line breakage	4,560
Customer line breakage	20,128
HV cable breakage	32,957m
4. Pole-mounted transformers	1,039
Box transformers	93
Station transformers	15
Underground distribution room (flooded)	7
Office buildings	30
Death tolls	2

B. Water supply

Facility	Number
Checker dam	1
Purification plants	30
Service offices	12
Affected customers	360,000

C. Natural gas supply

Company name	Total pipeline length (km)	Damaged pipeline length (km)	Affected customers
Shin Chung	1,228	38	213,600
Shin Chang	870	182	72,600
Shin Lin	860	591	82,000
Shin Yun	173	12	6,900
Chu Ming	95	11	300

D. Gasoline supply

Gas Stations	12

E. Communication

Regular telephones	205,291
Cellular phones	284,500

F. Sewage

Waste water plants	5

G. Transportation

Facility	Number
Highway	
1. Stoppages	711
2. Bridges	
Seriously Damaged	11
Reinforcement required	30
Reassessment required	5
Railway	
1. Tunnels	4
2. Bridges	
Seriously damaged	3
Reinforcement required	7
3. Rails	6km
4. Embankment	3.6km
Offices	80
1. Harbors	1
2. Post offices	18

SURFACE RUPTURES ON THE CHELUNGPU FAULT

By dawn in the same morning immediately following the earthquake, many geologists rushed to the epicenter area to make reconnaissance surveys of surface fault ruptures. Soon it was

discovered that the Chelungpu fault had slipped almost continuously, although sinuously,
along its whole length, extending southward from Shihgang in the northern end to Tungtou in the southern end. Soon later, splays of NE-trending surface fault ruptures were found extending northeastward from Shihgang toward Cholan. The total length of surface ruptures was estimated at about 125km [4]. Figure 1 shows the location of the Chelungpu fault and the amount of slips along its length.

It was observed that there was large uplift with some left-lateral strike-slip movement at many outcrop locations [5,6]. This was consistent with the fault-plane solution obtained by first motion data and CMT inversion, as shown in Fig. 1. It is remarkable that the amount of slip increased persistently from several tens of centimeters near the southern end to almost ten meters at the northern end of the fault.

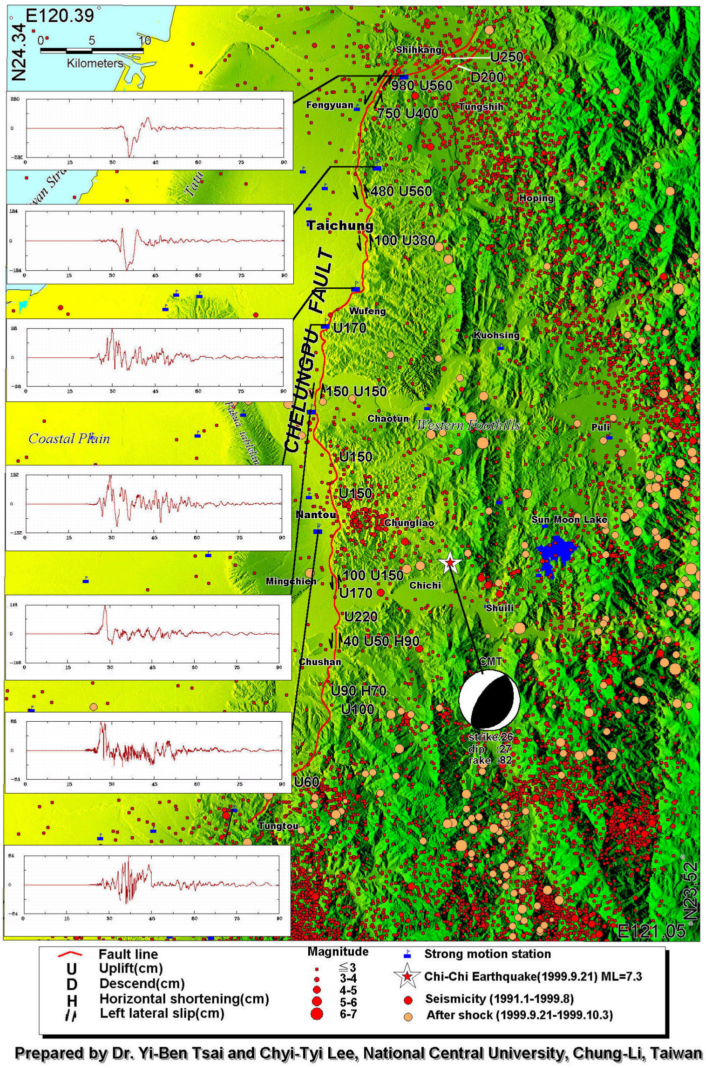

Fig. 1 The Chehlungpu fault, and the epicenter of the Chi-Chi earthquake. Also shown are background seismicity, strong aftershocks, E-W component velocity waveforms along the fault line

Figure 1 also shows the locations of background seismicity and strong aftershocks of the Chi-Chi earthquake. It is seen that most aftershocks took place far to the east of the Chelungpu fault in the curved zones of active background seismicity. Apparently, the zones of active background seismicity acted as the boundaries defining the slipped crustal block.

Figure 1 additionally shows several E-W component velocity waveforms integrated from original acceleration records obtained along the fault line. The apparent delays of the big pulse show that the fault rupture started from the hypocenter, and then propagated toward north and south. The average rupture velocity was about 2.5km/sec. The big velocity pulse at the northern end was significantly enhanced due to rupture directivity effects.

Figure 2 shows the regional geology of the epicenter area [6]. The Chelungpu fault clearly marks the boundary between the Pliocene formations in the east and Holocene alluvium west of the fault. An E-W cross section at the bottom of the figure shows a series of imbricate thrust faults dipping to the east. The Chelung-pu fault is just one of them.

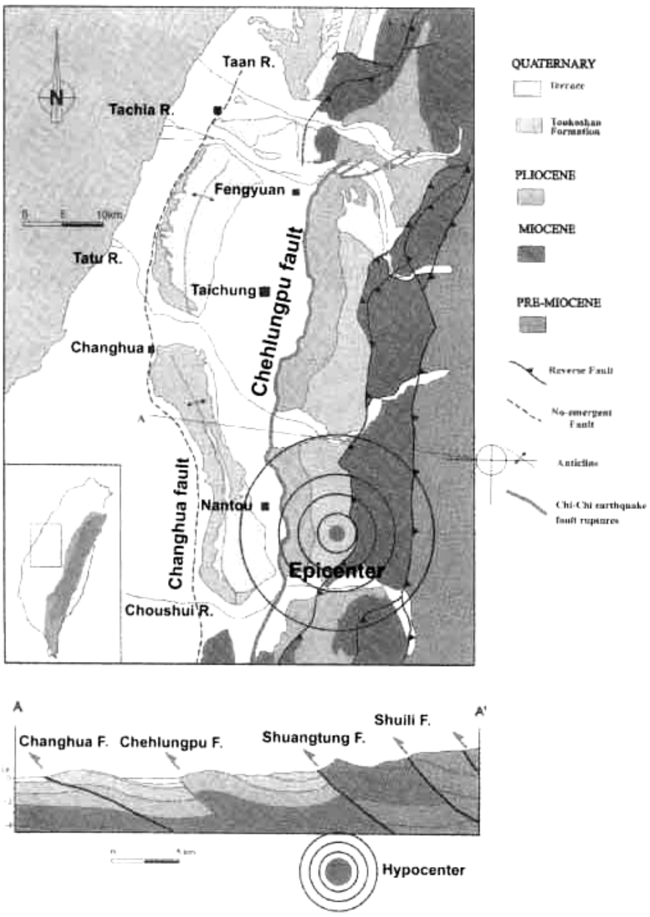

Fig. 2 Regional geology surrounding the Chehlungpu fault and an E-W cross section (after [6])

STRONG GROUND MOTION RECORDINGS

The Chi-Chi earthquake was well recorded by 422 free-field strong-motion accelerographs [3] of the TSMIP [7]. Figure 3 shows the locations of the recording sites on different geologic conditions. The recording sites have been classified into Classes B, C, D and E, according to geologic age [8]. Figure 4 shows that this new data set provides for the first time complete distance coverage for a M_W 7.7 earthquake. In the following we use the data set for three purposes: (1) To compare the observed peak ground acceleration (PGA) and peak ground velocity (PGV) data with several existing attenuation models. (2) To analyze the correlation of response spectral shapes with local geologic site conditions. (3) To study the near-fault effects on ground motion response spectra.

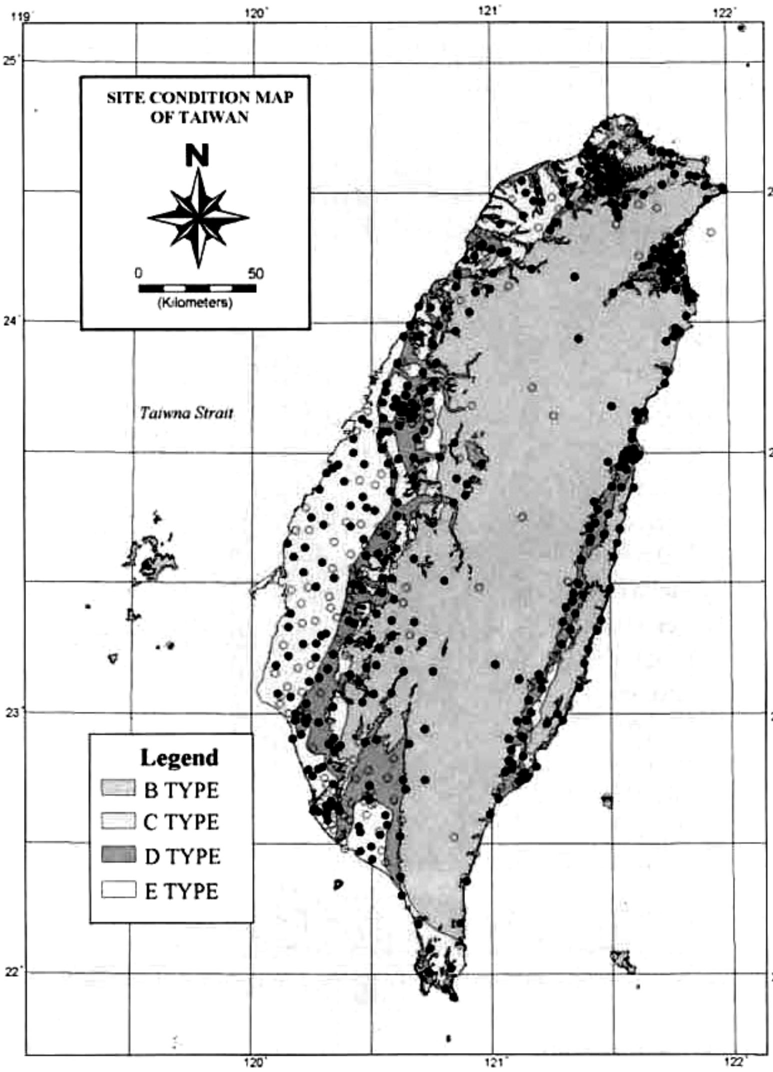

Fig. 3 Free-field strong motion accelerograph sites and geologic conditions of Taiwan

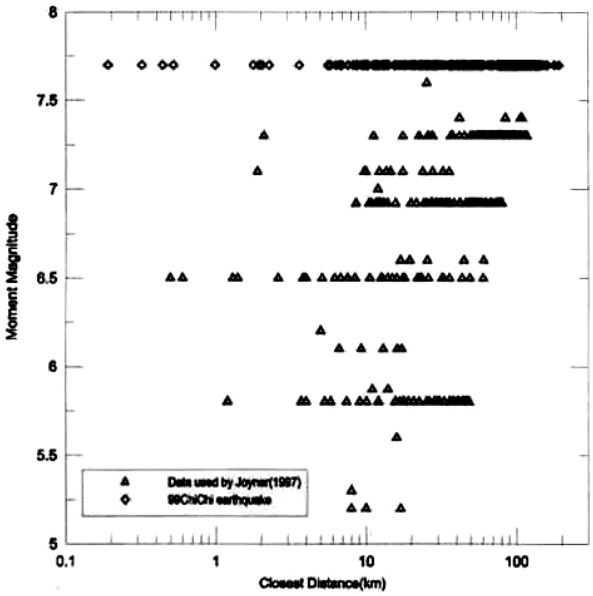

Fig. 4 The Chi-Chi, Taiwan earthquake produced a complete set of strong ground motion recordings for a large M7.7 shallow earthquake

ATTENUATION OF HORIZONTAL PEAK GROUND ACCELERATION

Figure 5 shows the recorded PGA values in g. It can be seen that the PGA values are significantly higher along the Chelungpu fault zone and in the hanging-wall areas to the east of the fault than in other areas. This was due to the event's thrust faulting mechanism that often caused stronger ground motions on the hanging wall block. This ground motion feature was closely correlated with the fatality rate in the epicenter area, as shown in Fig. 6.

In the following we compare the observed PGA data with several existing attenuation models. In Fig. 7 the observed horizontal PGA values are plotted as function of the closest distance to the seismogenic zone, according to Campbell's definition [9]. The data points are plotted separately according to the four site classes. In the same figure the data points from the Taipei Basin, Ilan Plain, and Hualien areas are also plotted separately. It is noted that the PGA values for Classes B, C, D and E sites are well mixed. However, the PGA values from the Taipei Basin, Ilan Plain, and Hualien areas are significantly higher than the rest of the data set. This was probably due to basin amplification.

In the figure we also plot the Campbell's median and median +/− one standard deviation curves for PGA from a M_W 7.7 thrust earthquake after having being scaled by a factor of 0.532 to match the data points. This shows that the observed PGA values from the earthquake are significantly lower than the worldwide average of the same magnitude earthquake. From the figure we can also see the slope of Campbell's curves follows quite well with the general trend of data points from the Chi-Chi earthquake.

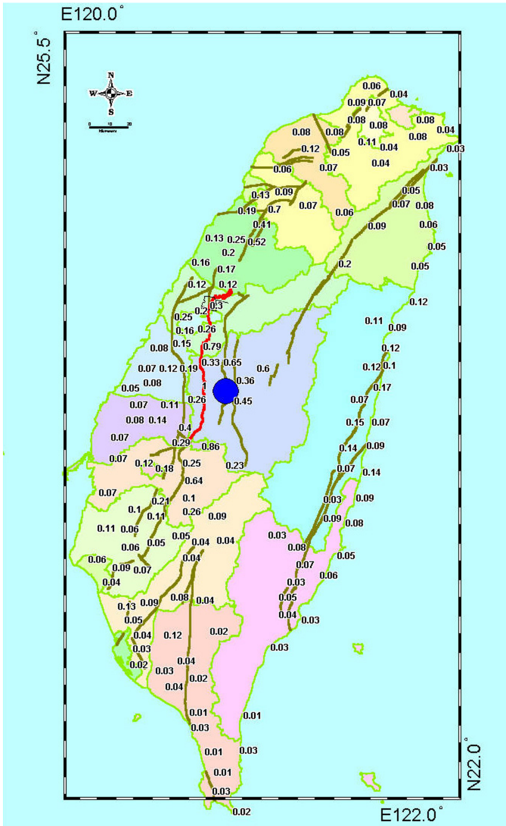

Fig. 5 Recorded horizontal peak ground acceleration values from the Chi-Chi, Taiwan earthquake of September 21, 1999

Fig. 6 Correlation of fatalities and recorded peak ground accelerations in central

Tausan from the Chi-Chi earthquake

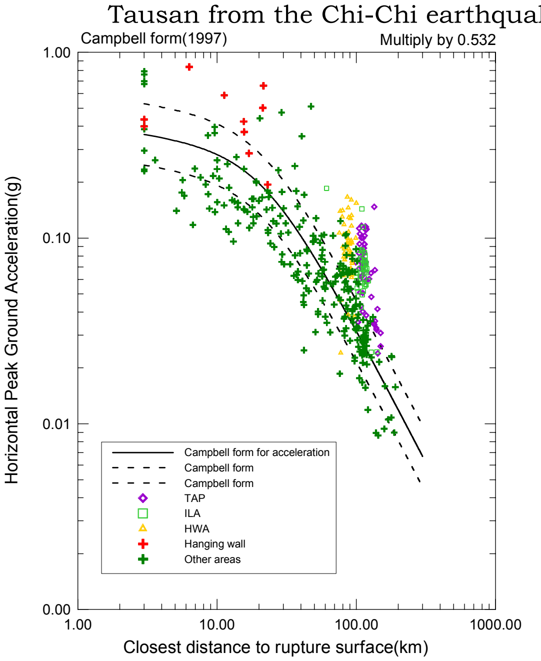

Fig. 7 Comparison of observed horizontal peak ground acceleration data from the Chi-Chi earthquake with the 1997 Campbell's attenuation model. Data from different site classes are marked separately

However, the data scattering is large in the distance range less than 20km. This was mainly due to several high PGA data points in the hanging wall area, as shown in Fig. 8. Similar patterns were observed previously from the 1995 Northridge, California earthquake [10].

Figure 9 shows a plot of horizontal PGA values as function of the closest distance to the surface projection of fault plane, according to the definition of Boore, *et al.*, [11]. The data points are plotted separately, according to the four site classes. Again, the data points from the Taipei Basin, Ilan Plain, and Hualien areas are also plotted separately. In the figure we also plot the Boore, *et al.*'s median and median +/− one standard deviation curves for PGA on soil sites from a M_W 7.7 thrust earthquake after having being scaled by a factor of 0.407 to match

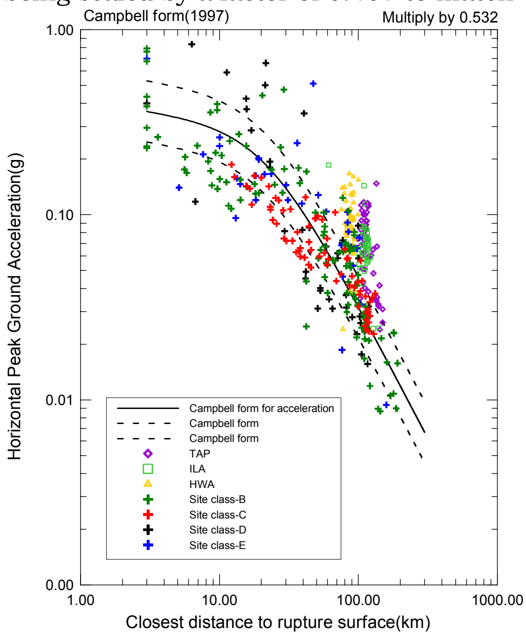

Fig. 8 Comparison of observed horizontal peak ground acceleration data from the Chi-Chi earthquake with the 1997 Campbell's attenuation model. Data from the hanging wall block are marked separately

the data points. We pick the soil curve because most of our recording sites are on soil.

From the figure we can see the slope of Boore, *et al.*'s curves follows quite well with the general trend of data points from the Chi-Chi earthquake. However, the observed PGA values from the Chi-Chi earthquake are significantly smaller than what would be predicted by the Boore, *et al.*'s attenuation curve for the same magnitude. In this case the data scattering at close-in distances is slightly improved due to the way the site distance is defined, as shown in Fig. 10. Again, the PGA values for Taipei Basin are apparently higher than the rest of the

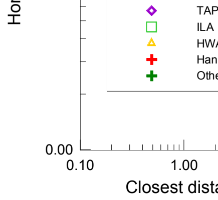

data set. On the other hand, the PGA values for Ilan Plain and Hualien area are not standing out now, due to change in the distance definition.

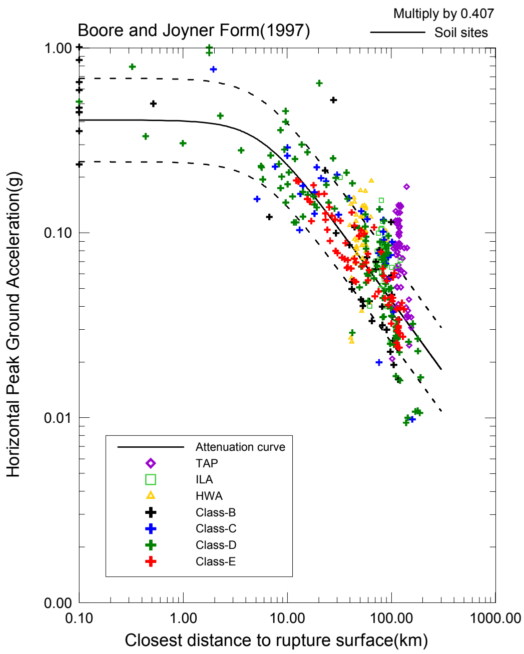

Fig. 9 Comparison of observed horizontal peak ground acceleration data from the Chi-Chi earthquake with the 1997 Boore, *et al.*'s attenuation model. Data from different site classes are marked separately

Fig. 10 Comparison of observed horizontal peak ground acceleration data from the Chi-Chi earthquake with the 1997 Boore, *et al.*'s attenuation model. Data from the hanging wall block are marked separately.

Figure 11 shows a plot of observed horizontal PGA values as function of the closest distance to the fault rupture surface, according to the definition of Sadigh, *et al.* [12]. The data points are plotted separately, according to the four site classes. In the meantime, the data points from the Taipei Basin, Ilan Plain, and Hwalien areas are plotted separately. In the figure we also plot the Sadigh, *et al.*'s median and median +/− one standard deviation curves for PGA on soil sites from a M_W 7.7 thrust earthquake after having been scaled by a factor of 0.384 to match the data points.

From the figure we can see the slope of Sadigh, *et al.*'s curves follows quite well with the general trend of data points from the Chi-Chi earthquake. However, the observed PGA values from the Chi-Chi earthquake are substantially below what would be predicted by Sadigh, *et al.*'s attenuation model for the same magnitude. In this case the data scattering at close-in distances is large mainly due to data points in the hanging wall area, as shown in Fig. 12. The observed PGA values for the Taipei Basin, Ilan Plain, and Hwalien areas are apparently higher than the rest of the data set.

In summary, we found that the observed horizontal PGA values from the Chi-Chi earthquake were only 0.532, 0.407 and 0.384 times what would be predicted for the same magnitude from Campbell's, Boore, *et al.*'s and Sadigh, *et al.*'s attenuation models. Conversely, the observed horizontal PGA values are equivalent to what would be predicted

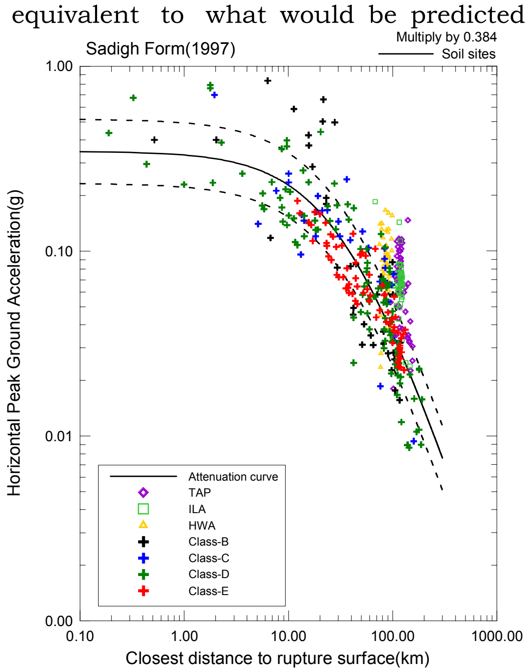

Fig. 11 Comparison of observed horizontal peak ground acceleration data from the Chi-Chi earthquake with the 1997 Sadigh ’s attenuation model. Data from different site classes are marked separately

Fig. 12 Comparison of observed horizontal peak ground acceleration data from the Chi-Chi earthquake with the 1997 Sadigh’s attenuation model. Data from the hanging wall block are marked separately

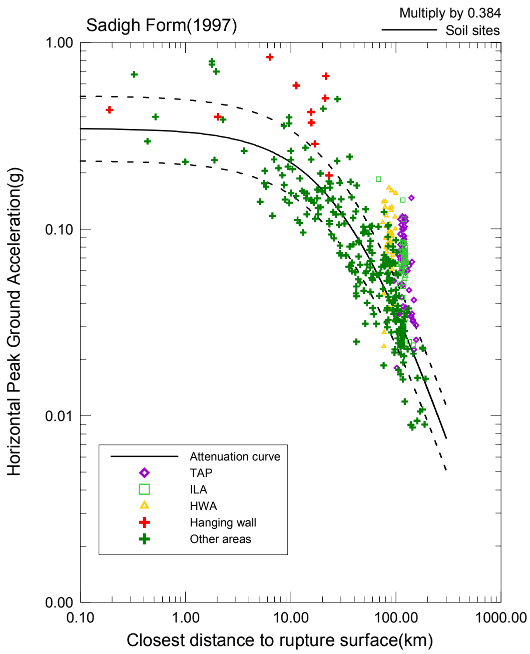

for M_W 6.6, 6.0, and 6.2 from Campbell’s, Boore, *et al.*’s, and Sadigh, *et al.*’s attenuation models, respectively. Thus, the observed horizontal PGA values from the Chi-Chi earthquake are significantly lower than the worldwide average PGA value of similar magnitude earthquakes. This partly explains why the damage in the epicenter areas, in particular in the densely populated areas west of the Chelungpu fault, was not more severe than what had happened. The observed horizontal PGA values at Taipei Basin, Ilan Plain and Hwalien areas are significantly higher than the other areas. This apparently explains why the damage in the Taipei Basin area was quite widespread.

ATTENUATION OF VERTICAL PEAK GROUND ACCELERATION

In Fig. 13 we plot the observed vertical PGA values as function of the closest distance to the seismogenic zone, according to Campbell’s definition [9]. The data points are plotted according to the four site classes. In the same figure the data points from the Taipei Basin, Ilan Plain, and Hualien areas are plotted separately. It is noted that the vertical PGA values for Classes B, C, D and E sites are well mixed. However, the vertical

PGA values from the Taipei Basin, Ilan Plain, and Hualien areas are significantly higher than the rest of the data set. This was probably due to basin amplification.

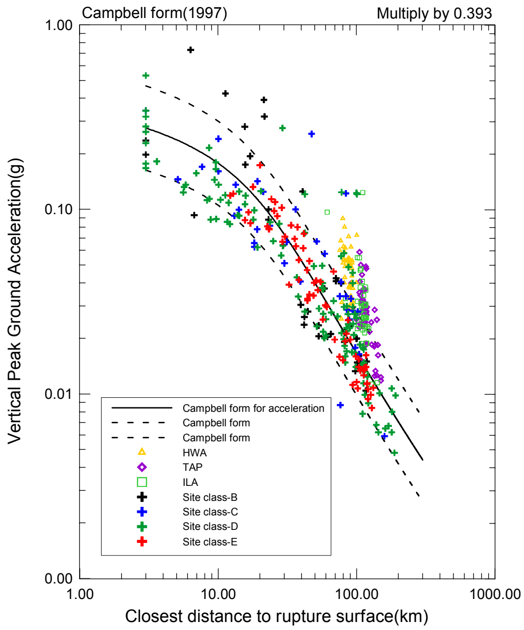

Fig. 13 Comparison of observed vertical peak ground acceleration data from the Chi-Chi earthquake with the 1997 Campbell's attenuation model. Data from different site classes are marked separately.

In the figure we also plot the Campbell's median and median +/– one standard deviation curves for PGA from a M_W 7.7 thrust earthquake after having been scaled by a factor of 0.393 to match the data points. This means that the observed vertical PGA values from the earthquake are significantly lower than the worldwide average of the same magnitude earthquakes. From the figure we can also see the slope of Campbell's curves follows quite well with the general trend of data points from the Chi-Chi earthquake. However, the data scattering is large in the distance range less than 20km. This was mainly due to several high PGA data points in the hanging wall area, as shown in Fig. 14. By comparing Figs. 7 and 13 it is found that the vertical

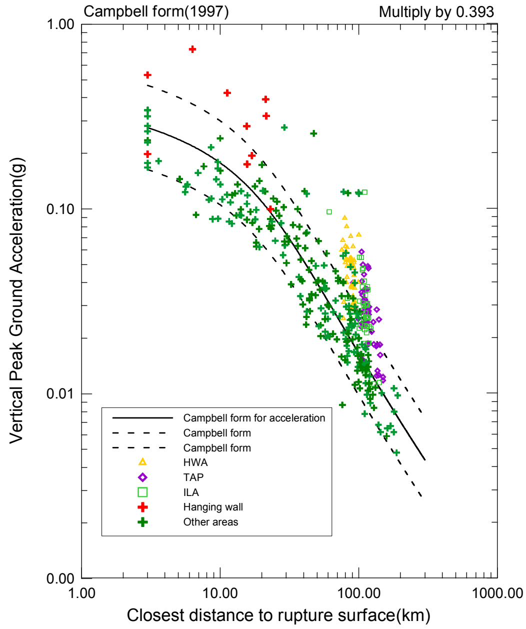

Fig. 14 Comparison of observed vertical peak ground acceleration data from the Chi-Chi earthquake with the 1997 Campbell's attenuation model. Data from the hanging wall block are marked separately.

PGA values in general are about 0.6 times the corresponding horizontal PGA values.

ATTENUATION OF PEAK GROUND VELOCITY

Figure 15 shows the geographical distribution of the integrated horizontal peak ground velocity (PGV) values in cm/sec. It can be seen that the PGV values are not significantly higher along the Chelungpu fault zone and the hanging wall areas to the east than in other areas. The asymmetric patterns due to thrust faulting mechanism are not apparent for low-frequency velocity waveforms.

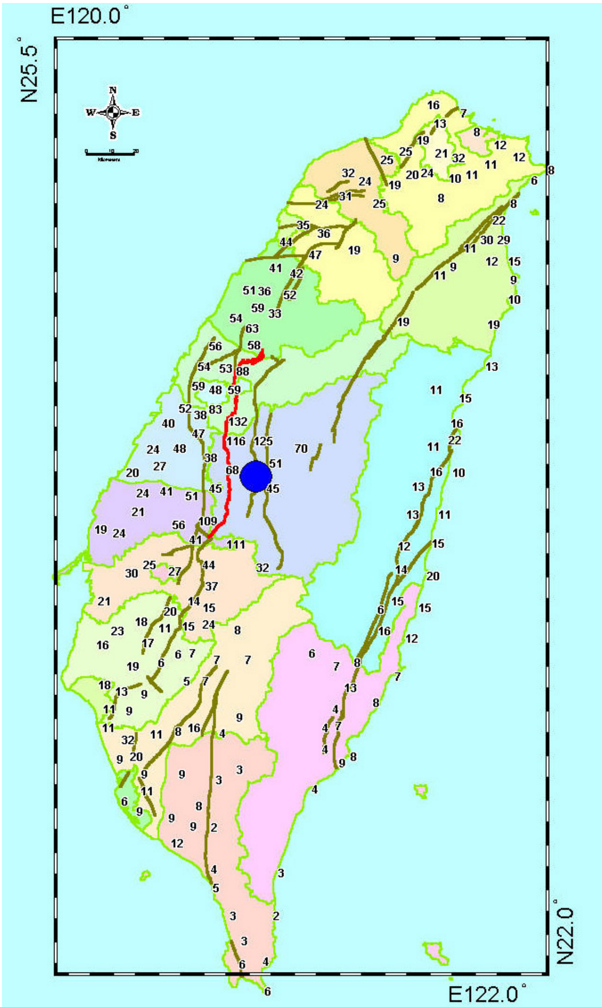

Fig. 15 Distribution of integrated horizontal peak ground velocity

Figure 16 plots the observed horizontal PGV values from Class B, C, D, E sites as function of the closest distance to the seismogenic zone, according to Campbell's definition [9]. In the figure we also plot the median and median +/− one standard deviation curves predicted for M_W 7.7 from Campbell's attenuation model after having been scaled by a factor of 1.876 in order to fit the data points. Unlike the PGA values, the observed horizontal PGV values from the Chi-Chi earthquake are significantly higher than the worldwide average of the same magnitude earthquake.

The slope of the Campbell's curves follows quite closely with the general trend of data points. The data scattering at close-in distances is not more than at greater distances. This confirms the absence of asymmetric patterns of PGV due to thrust faulting mechanism. Furthermore, It can be seen from the figure that the data points from all four different site classes are well mixed. However, the observed horizontal PGV values from Taipei Basin, Ilan Plain, and Hwalien areas are apparently higher than the rest of the data set.

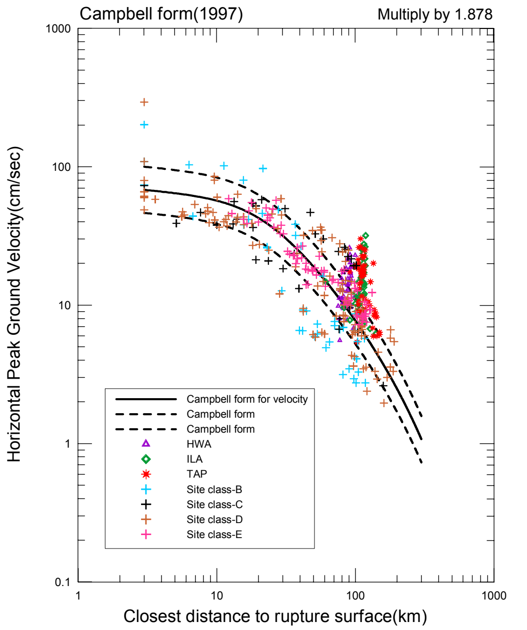

Fig. 16 Comparison of observed horizontal peak ground velocity data from the Chi-Chi earthquake with the 1997 Campbell's attenuation model. Data from different site classes are marked separately

CORRELATION OF GROUND ACCELERATION RESPONSE SPECTRUM SHAPE WITH LOCAL SITE CONDITIONS

In the following we analyze the 5% damped acceleration response spectrum shapes for four different site classes B, C, D, and E in order to study possible dependence of response spectrum shape on local site conditions. For the sake of easy comparison, we use four modified seismic design spectra for Types 1, 2, 3 and Taipei Basin sites, respectively. They are obtained by replacing the constant value of 1.0 at long periods (T) on current seismic design spectra in the Taiwan Building Code (TBC) with a 1/T function. In addition, the amplification factor is increased from 2.0 to 2.5 for the modified design spectrum for Taipei Basin in current Taiwan Building Code (TBC).

Figure 17 shows the normalized response spectrum shape for Class B sites on rocks of Miocene age or older, as well as the four modified seismic design spectra. The median curve has spectral amplification over periods up to about 1.5 seconds. It is similar to the modified seismic design spectrum for Type 2 sites in the current Taiwan Building Code (TBC). For periods greater than 1 second the observed median curve is clearly below the modified TBC spectrum level. The peak spectral amplification factor is about 2.3.

Figure 18 shows the normalized response spectrum shape for Class C sites on soft rocks of Pliocene or Pleistocene ages, as well as the four modified seismic design spectra. The median curve has spectral amplification over periods up to about 2.0 seconds. It is similar to the modified seismic design spectrum for Type 3 sites in the current Taiwan Building Code (TBC). For periods shorter than 5 seconds the observed median curve follows closely with the modified Type 3 spectrum. The peak spectral amplification factor is about 2.4.

Figure 19 shows the normalized response spectrum shape for Class D sites on stiff soils of late Pleistocene age or younger, as well as the four modified seismic design spectra. The median curve has spectral amplification over periods up to about 1.7 seconds. It is similar to the modified seismic design spectrum for Type 3 sites in the current Taiwan Building Code (TBC). For periods greater than 1.5 seconds the observed me-dian curve is clearly below the modified TBC Type 3 spectrum level. The peak spectral amplification factor is about 2.3.

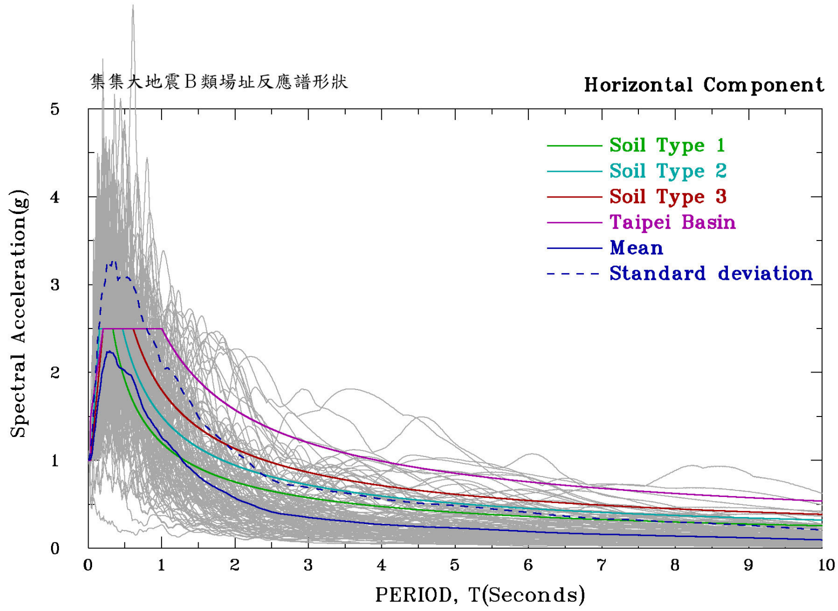

Fig. 17 Comparison of the normalized 5% damped acceleration response spectra from Class B sites with the modified Type 1, 2, 3 and Taipei Basin seismic design spectra

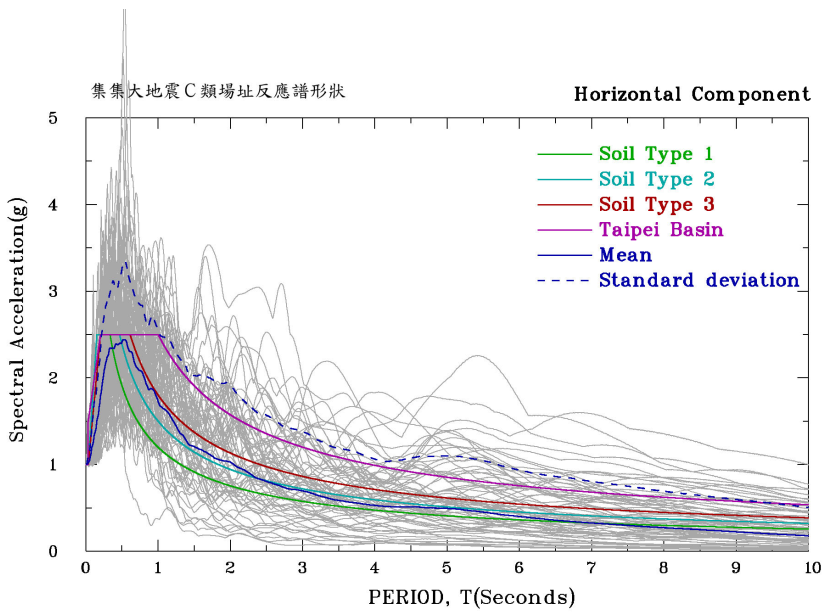

Fig. 18 Comparison of the normalized 5% damped acceleration response spectra from Class C sites with the modified Type 1, 2, 3 and Taipei Basin seismic design spectra

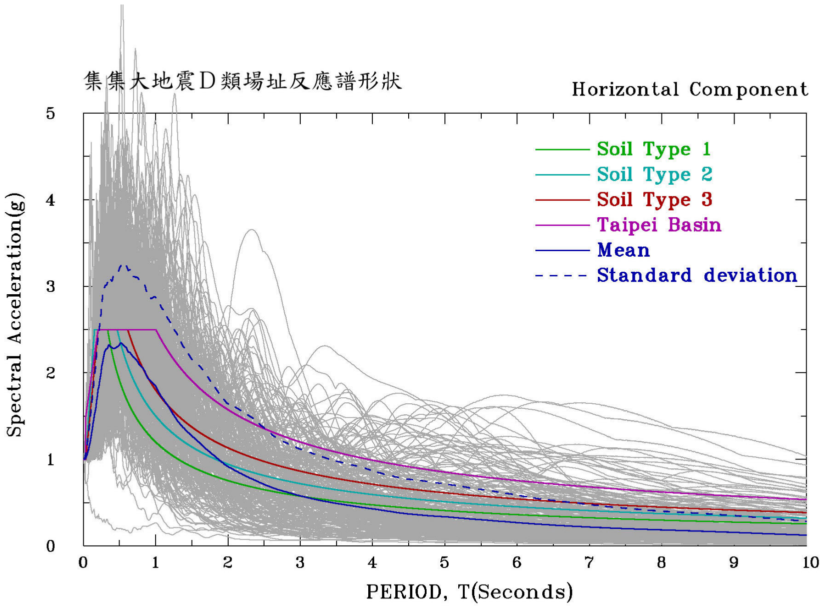

Fig. 19 Comparison of the normalized 5% damped acceleration response spectra from Class D sites with the modified Type 1, 2, 3 and Taipei Basin seismic design spectra

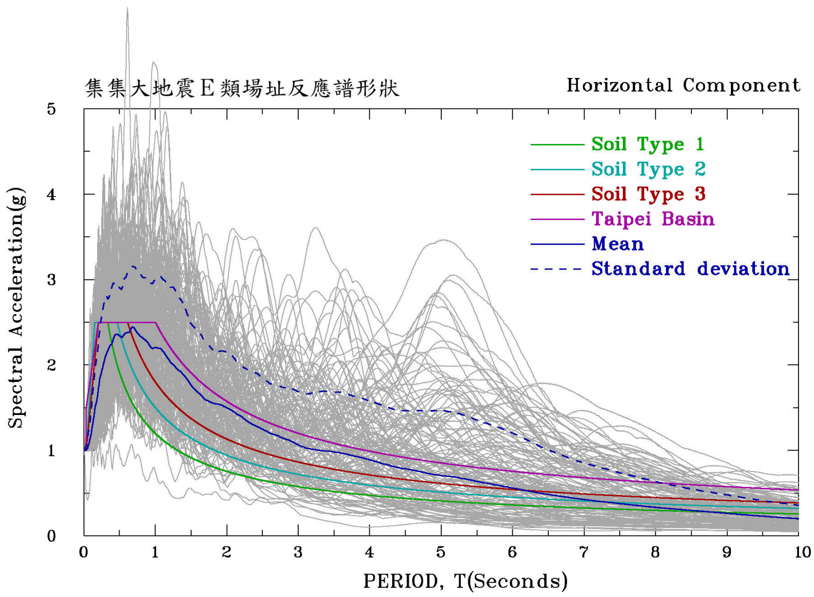

Fig. 20 Comparison of the normalized 5% damped acceleration response spectra from Class E sites with the modified Type 1, 2, 3 and Taipei Basin seismic design spectra

Figure 20 shows the normalized response spectrum shape for Class E sites on soft soils of late Pleistocene age or younger, as well as the four modified seismic design spectra. The median curve has spectral amplification over periods up to about 3.0 seconds. It follows closely but falls slightly below the modified seismic design spectrum for Taipei Basin sites in the current Taiwan Building Code (TBC). For periods greater than 4.0 seconds the observed median curve deviates more below the modified TBC Taipei Basin spectrum level. The peak spectral amplification factor is about 2.4.

In summary, we have seen clear dependence of response spectrum shape on local geologic site conditions from the recordings of the Chi-Chi earthquake. The median spectrum shape of Class B sites is similar to the modified Type 2 seismic design spectrum in current TBC. The median spectrum shapes of Classes C and D sites are similar to the modified Type 3 seismic design spectrum in current TBC. Finally, the median spectrum shape of Class E sites is similar to the modified Taipei Basin seismic design spectrum in current TBC.

NEAR-FAULT GROUND ACCELERATION RESPONSE SPECTRA

Finally, we analyze the observed acceleration response spectra from 64 near-fault sites to study their characteristics. Figure 21 shows the response spectra for the 9 sites within 2km from the surface fault ruptures. The median response spectrum has a horizontal PGA value of about 0.5g and a corresponding spectral peak of about 1.0g. The mediam-

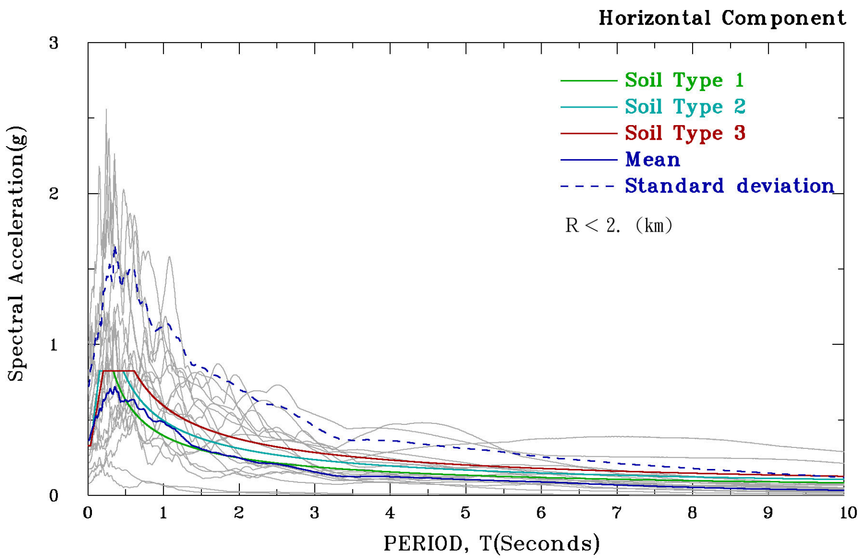

Fig. 21 Comparison of 5% damped response acceleration spectra from the recording sites within 2km of the Chehlungpu fault with the modified seismic design spectra anchored at 0.33g

plus-one-standard-deviation horizontal PGA value is about 0.7g and the corresponding spectral peak is about 1.8g. In the figure are shown the three modified TBC seismic design spectra anchored at a PGA of 0.33g. It is found that the median curve for sites located within 2km of the surface fault ruptures matches well with the Type 3 design spectrum, except at very short periods. Thus, with a scaling factor of 1.5 applied to the current seismic design spectrum anchored at a PGA value of 0.33g for Zone 1A appears to be conservative, as shown in Fig. 22.

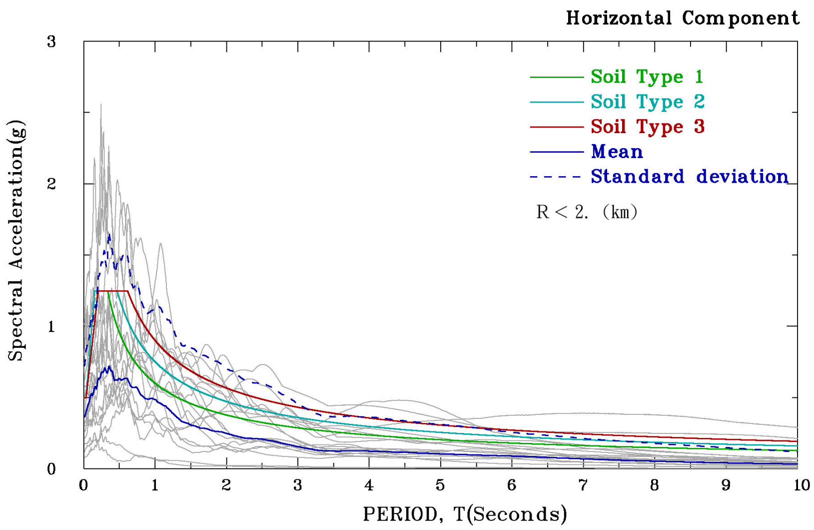

Fig. 22 Comparison of 5% damped response acceleration spectra from the recording sites within 2km of the Chehlungpu fault with the modified seismic design spectra anchored at 0.50g

Figure 23 shows the response spectra for the 21 sites located at 2 to 10km from the surface fault ruptures. The median horizontal PGA value is about 0.25g and the corresponding peak spectral value is about 0.6g. The median-plus-one-standard-deviation horizontal PGA value is about 0.4g and the corresponding peak spectral value is about 0.8g. Thus, for sites located between 2 and 10km from the surface fault ruptures the current seismic design spectrum anchored at a PGA value of 0.33g for Zone 1A appears to be more than adequate.

Figure 24 shows the response spectra for the 34 sites located at 10 to 20km from the surface fault ruptures. The median horizontal PGA value is about 0.18g with a corresponding peak spectral value of about 0.45g. The median-plus-one-standard-deviation horizontal PGA value is about 0.3g with a corresponding peak spectral value of about 0.7g. Thus, for sites located between 10 and 20km from the surface fault ruptures the current seismic design spectrum anchored at a PGA value of 0.33g for

Zone 1A is much more than adequate.

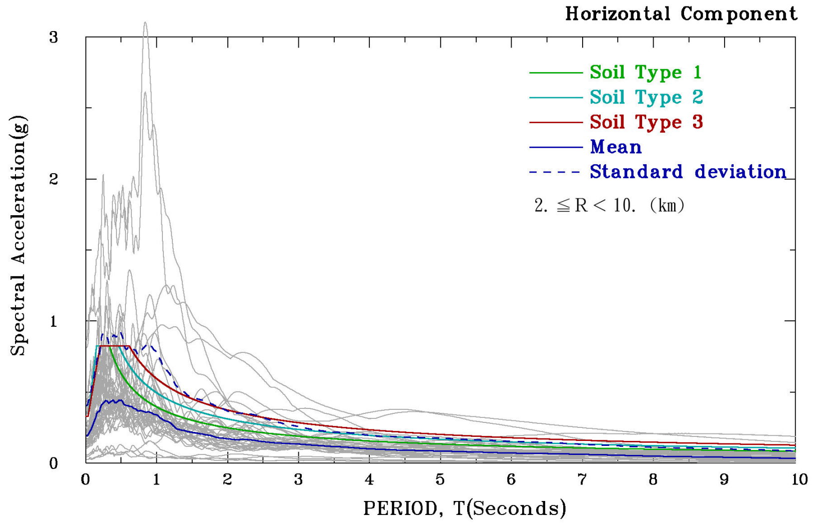

Fig. 23 Comparison of 5% damped response acceleration spectra from the recording sites at 2 to 10km of the Chehlungpu fault with the modified seismic design spectra anchored at 0.33g

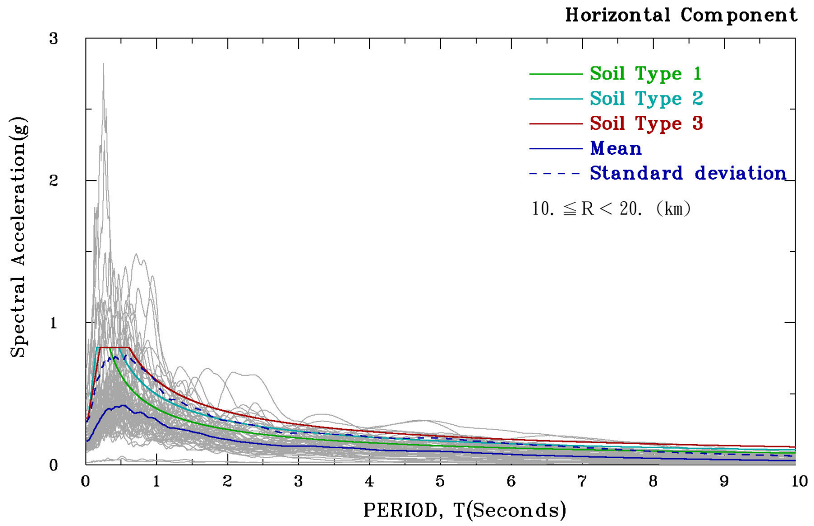

Fig. 24 Comparison of 5% damped response acceleration spectra from the recording sites at 10 to 20 km of the Chehlungpu fault with the modified seismic design

spectra anchored at 0.33g

CONCLUSIONS

The Chi-Chi, Taiwan earthquake produced a rich set of 422 strong ground motion recordings for a large earthquake of M_W 7.7. We have analyzed this set of data to gain some insights of the characteristics of strong motions caused by this disastrous earthquake. The results are summarized below.

First, we analyzed the observed horizontal PGA values from the earthquake. We found the overall level of PGA values was relatively low (about 50% less) when compared with what would be predicted for an earthquake of the same magnitude by several existing attenuation models based on worldwide data. The high horizontal PGA values at sites on the hanging wall and within 20km of the surface fault ruptures are notable exceptions. The horizontal PGA values at four different site classes are indistinguishable. But the horizontal PGA values in Taipei Basin, Ilan Plain, and Hwalien areas are apparently higher than other areas at similar distances. The vertical PGA values on the average are about 0.6 times their horizontal counterparts.

Unlike the horizontal PGA, the observed horizontal PGV values are relatively high (about 80% higher) when compared with what would be predicted for an earthquake of the same magnitude by an existing PGV attenuation model based on worldwide data. In summary, as far as peak ground motion parameters are concerned, the Chi-Chi earthquake may be called a high-PGV, but low-PGA (HV-LA) earthquake.

Next, we analyzed the 5% damped acceleration response spectrum shapes for four different site classes B, C, D, and E in order to study possible dependence of response spectrum shape on local site conditions. It is found that the peak spectral amplification factor ranges between 2.3 and 2.5 for all four classes of site conditions. In general, the response spectrum shape for Class B sites on soft rocks older than Pliocene age has spectral amplification over periods up to about 1.5 seconds. The spectral amplification of Classes C and D sites on stiff soils occurs over periods up to about 2.0 seconds. The spectral amplification of Class E sites on soft soils occurs over periods up to about 3.0 seconds. The response spectrum shapes for Taipei Basin and Ilan Plain are similar to Class E sites, whereas Hwalien area is similar to Class C or D sites.

Finally, we analyzed the observed acceleration response spectra from 64 near-fault sites to study their characteristics. For the 9 sites located within 2km from the surface fault ruptures the median horizontal PGA value is about 0.5g with a corresponding spectral peak of about 1.0g. The median-plus-one- standard-deviation horizontal PGA value is about 0.7g with a corresponding spectral peak of about 1.8g. Thus, for sites located within 2km of the surface fault ruptures a scaling factor of 1.5 applied to the current seismic design spectrum anchored at a PGA value of 0.33g for Zone 1A appears to be appropri- ate.

For the 21 sites located at 2 to 10km from the surface fault ruptures, the median horizontal PGA value is about 0.25g with a corresponding peak spectral value of about 0.6g. The median-plus-one-standard-deviation horizontal PGA value is about 0.4g with a corresponding peak spectral value of about 0.8g. Thus, for sites located between 2 and 10km from the surface fault ruptures the current seismic design spectrum anchored at a PGA value of 0.33g for

Zone 1A appears to be adequate.

For the 34 sites located at 10 to 20km from the surface fault ruptures, the median horizontal PGA value is about 0.18g with a corresponding peak spectral value of about 0.45g. The median-plus-one-standard-deviation horizontal PGA value is about 0.3g, with a corresponding peak spectral value of about 0.7g. Thus, for sites located between 10 and 20km from the surface fault ruptures the current seismic design spectrum anchored at a PGA value of 0.33g for Zone 1A is more than adequate.

ACKNOWLEDGEMENTS

The materials of this paper were presented previously at the International Workshop on Chi-Chi, Taiwan Earthquake of September 21, 1999, held on December 14~17, 1999 in Taichung, Taiwan. The strong ground motion recordings were provided by the Central Weather Bureau. We sincerely thank the people who maintained the instruments. We also would like to thank Dr. C.T. Lee and Mr. C.T. Cheng for providing the TSMIP site classification information before publication. This research was supported by the National Science Council under Contract No. NSC 89-2625-2- 008-007.

REFERENCES

1. Chang, C.H., Wu, Y.M., Shin, T.C., Wang, C.Y. and Hsiao, N.C. (1999). "A study of initial rupture of the Chi-Chi, Taiwan earthquake," *Proceedings of the Special Session on the Chi-Chi, Taiwan earthquake at the 1999 Annual Meeting of the Chinese Geophysical Society*, in Chinese, pp. 1–6.
2. National Post-Earthquake Reconstruction Steering Commission (1999). "Report on the disasters of the September 21, 1999 earthquake and their management," in Chinese, 18p.
3. Shin, T.C., Kuo, K.W., Lee, W.H.K., Teng, T.L. and Tsai, Y.B. (1999). "A preliminary report on the 1999 Chi-Chi (Taiwan) earthquake," *Seism. Res. Lett.*, submitted.
4. Ma, K.F., Lee, C.T. and Tsai Y.B. (1999). "The Chi-Chi, Taiwan earthquake: Large surface displacements on an inland thrust fault," *EOS, Transactions*, AGU, Vol. 40, pp. 605–611.
5. Huang, C.Y. (1999). "Seismic geology of the Chi-Chi earthquake," *Proceedings of the International Workshop on Chi-Chi, Taiwan Earthquake of September 21, 1999*, pp. 3-1–3-20.
6. Lee, C.T. (1999). "Results of field geologic investigations of the Chi-Chi earthquake," personal communication.
7. Liu, Kun-Sung, Shin, Tzay-Chyn and Tsai, Yi-Ben (1999). "A free-field strong motion network in Taiwan: TSMIP," *TAO*, 10, pp. 377–396.
8. Lee, C.T. and Cheng, C.T. (1999). "Geologic classification of the free-field strong-motion accelerograph sites of TSMIP," personal communication.
9. Campbell, K.W. (1997). "Empirical near-source attenuation relationships for horizontal and vertical components of peak ground acceleration, peak ground velocity, and pseudo-absolute acceleration response spectra," *Seism. Res. Letter*, 68, pp. 154–179.
10. Abrahamson, N.A. and Somerville, P.G. (1996). "Effects of the hanging wall and footwall on ground motions recorded during the Northridge Earthquake," *Bull. Seism. Soc. Am.*, 86, pp. S93–S99.
11. Boore, D.M., Joyner, W.B. and Fumal, T.E. (1997). "Equations for estimating horizontal response spectra and peak acceleration from western north American earthquakes: A summary of

recent work," *Seism. Res. Letter*, 68, pp. 128– 153.

12. Sadigh, K., Chang, C.Y., Egan, J.A., Makdisi, F. and Youngs, R.R. (1997). "Attenuation relationships for shallow crustal earthquakes based on California strong motion data," *Seism. Res. Letter*, 68, pp. 180–189.